PAPER • OPEN ACCESS

Comparative assessment of actuator-Line modeling of FOWT rotor aerodynamics to wind tunnel experiments

View the article online for updates and enhancements.

Comparative assessment of actuator-Line modeling of FOWT rotor aerodynamics to wind tunnel experiments

Andrea G Sanvito[1], Giacomo Persico[1], Paolo Schito[2], Vincenzo Dossena[1], Alberto Zasso[2]

[1] Laboratory of Fluid-Machines, Department of Energy, Politecnico di Milano, Via Lambruschini 4, 20156 Milano, Italy
[2] Department Mechanical Engineering, Politecnico di Milano, Via La Masa 1, 20156 Milano, Italy

E-mail: andreagiuseppe.sanvito@polimi.it

Abstract. The paper presents aerodynamic analyses of the scaled DTU 10MW laboratory model with surge and pitch platform motion in controlled environment applying an Actuator Line Method (ALM) to reproduce the experiments conducted in the large-scale Wind Tunnel of the Politecnico di Milano during UNAFLOW and OC6 Phase III test campaigns. The Effective Velocity Method (EVM) is implemented in the in-house ALM solver to sample the velocity at actuator points and determine the angle of attack. Fixed-bottom wind turbine URANS simulations reveal that thrust and torque deviations are within 3% and 5% respectively to experimental counterparts. Platform surge and pitch are simulated with ALM adopting a combination of motion frequencies and amplitudes finding a good agreement with experimental counterparts both in terms of loads and wake quantities. This paper also shows the capability of in-house ALM to model control strategies, imposing sinusoidal variation of blade collective pitch, which might generate dynamic inflow conditions. An in-depth cross comparison is conducted on FOWT wake quantities to investigate the flow behaviour and wake recovery induced by floating motion.

1. Introduction

The challenge to find better wind source conditions for multi-MegaWatt gargantuan wind turbines unleashed the great potential of offshore sites with fixed-bottom wind turbines, in shallower waters, and Floating Offshore Wind Turbines (FOWTs) for sea beds deeper than 50 m. The stronger and more constant winds in open sea help improve the capacity factor and promote the reduction of Levelized Cost of Energy (LCoE). Abatement of LCoE is also pursued increasing the density of installed power by the wind farms, to this aim the wake recovery and mixing are essential to preserve, and increase, the wind farm efficiency jeopardized by wind turbine interactions with upstream wakes. Multi-fidelity numerical tools investigate FOWTs whose full-scale experimental assessment is economically and logistically unfeasible. Validation of the numerical tools is the first step towards multi-objective wind farm optimisation which has to rely on engineering models to manage the wide complexity of such a interdisciplinary matter.

In this paper, a wide comparison of a scaled laboratory model to the wind tunnel tests is provided in terms of key turbine parameters and wake quantities in floating operations. The focus
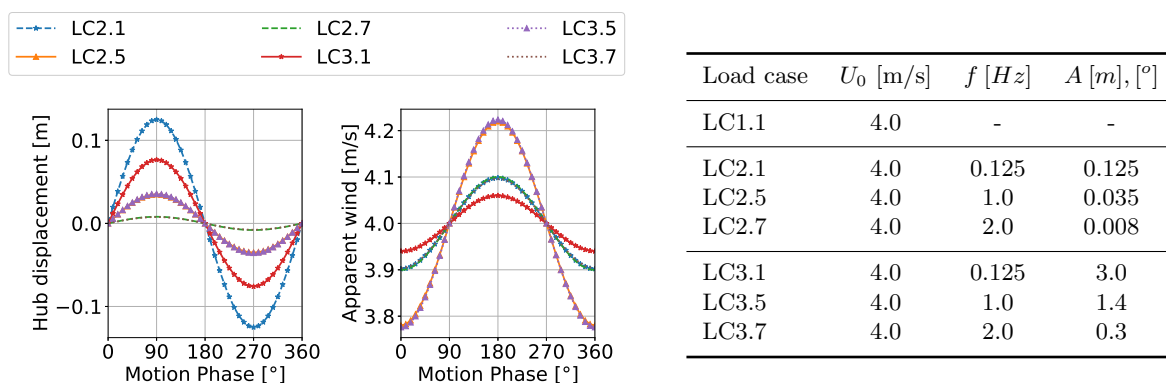
of this paper is the numerical simulation of FOWTs in the wind tunnel controlled environment employing the ALM. The in-house ALM inherits the treatment of the rotor aerodynamics from the Blade Element Moment Theory (BEMT) and solves Navier-Stokes equations in each elementary discretised volume like CFD tool. This was originally proposed by Sørensen [1] for HAWTs and validated for turbulent inflows in [2] and [3]. Several studies have been published on actuator line modelling of HAWTs, however applications on floating structures are limited to studies in [4], [5]. ALM results of DTU 10 MW scaled model were provided in [6] and available in OC6 Phase III [7]. This scientific work uniquely contributes with an experimental comparison of CFD-ALM using CFD URANS solver with prescribed floating platform motions describing thoroughly the CFD set-up for the repeatability of the test cases.

2. Experimental measurements

The experimental validation has been carried out in GVPM [8] for UNAFLOW project [9], [10] and OC6 Phase III (IEA Task 30) [6] with the DTU 10 MW 1:75 scaled wind turbine model [11]. The 2.38m-diamater rotor rotates at 240 rpm for the case analysed, the nose of nacelle has a hub radius of 0.089 m, no tilted rotor is considered and the density measured in the wind tunnel is $\rho = 1.177\ kg/m^3$. The wind tunnel cross section dimensions ($13.84 \times 3.84\ m$), whilst the tested free stream velocity has been scaled with 1:3 ratio to avoid laminar to turbulent phenomena originated by low Reynolds numbers, ranging from 50k to 200k. The low-Reynolds SD7032 airfoil shape has a twist and tapered chord distribution along the span and a profile is tested in a 2D wind tunnel to characterise the aerodynamic coefficients [10]. Experimental layouts of surge and test campaign are reported in [12], The positive platform motion is aligned with the windward direction. Surge experimental and numerical platform motions are imparted as negative sinusoidal displacement whereas the pitch platform motion has an opposite direction. Set-up parameters adopted in UNAFLOW project and OC6 Phase III details on experimental campaigns are expanded in [10] and [6].

2.1. Test cases

The numerical validation is pursued by testing the wind turbine in the fixed-bottom configuration and in FOWT operations with a combination of amplitudes and frequencies reported in Tab.1. The wind turbine floating motion is imparted through hydraulic actuators resembling sinusoidal displacements as illustrated by Fig.1.

Load case	U_0 [m/s]	f [Hz]	A [m], [°]
LC1.1	4.0	-	-
LC2.1	4.0	0.125	0.125
LC2.5	4.0	1.0	0.035
LC2.7	4.0	2.0	0.008
LC3.1	4.0	0.125	3.0
LC3.5	4.0	1.0	1.4
LC3.7	4.0	2.0	0.3

Figure 1. Hub displacement velocity and apparent wind at hub height.
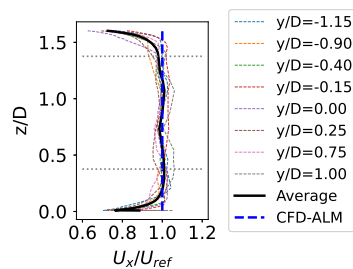
Table 1. Simulation matrix of UNAFLOW and OC6 Phase III load cases.

The apparent wind is defined as the relative wind speed experienced by the wind turbine in the absolute frame, it is given by the vectorial summation of the free stream wind speed and
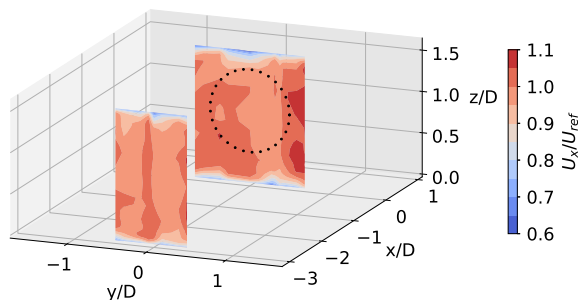
Figure 2. Normalized velocity at x/D=3 upstream and at rotor plane, rotor in black dotted line ($\cdots\cdots$).

Figure 3. Velocity profiles at x/D=3 upstream, y/D=0. Experiments: black solid line (——); ALM: dashed blue line (- - - -).

turbine velocity itself at hub height, here the assumption of perfect rigid dynamic response is ensured by the design of a stiff wind turbine tower. In Fig.1, the hub displacement along x-coordinate of the floating load cases is shown: load cases LCX.1 and LCX.7 have been designed to give the same apparent wind amplitude $\Delta V = 0.1$, nonetheless the hexapod robot had a constraint on the maximum oscillation allowed of 3°, so that LC3.1 has a lower apparent wind. Load case LCX.5, with surge and pitch frequency $f = 1\,Hz$, are characterized by an apparent wind twice the other's ones.

In the wind tunnel simulations the free stream wind speed $U_0 = 4$ m/s and the turbulence intensity is lower than 2% measured at $3D$ upstream the rotor. The development of the wind tunnel boundary layer and the presence of the rotor in the test section originate a blockage ratio of 8% [6]. Two velocity planes were measured at x/D=3 (upstream) and x/D=0 (rotor plane) without the presence of the turbine, in Fig.2 the velocity is normalized by the average velocity at hub height, U_{ref}. As the velocity profile is deemed constant in correspondence of the rotor, CFD stimulation adopts a flat, uniform wind profile equal to the free stream velocity measured during the test cases.

3. ALM solver
The ALM approach was formulated by Sørensen in 2002 [1], it stems from the application of the BEMT to the wind turbine rotor and a typical CFD solver for the surrounding fluid domain solving Navier-Stokes (NS) equations with the finite volume approach. The wind turbine blades is replaced by actuator lines (AL) constituted by AL points which represent the locations along the blade where aerodynamic forces are computed and then integrated to find overall turbine performances. Those forces contribute to the source term $\mathbf{f}$ of the NS momentum equation written in a condensed form in Eq.1. Pointwise forces are spread over the numerical domain by the convolution of 2D Gaussian spreading function η_ϵ^{2D} in Eq.2 to avoid singularity issues [3]. The spreading parameter ϵ indicates the size of the regularization kernel whereas d is the distance between a generic cell centre and the actuator line point.

$$\frac{\partial \mathbf{u}}{\partial t} + \mathbf{u} \cdot \nabla \mathbf{u} = -\nabla p + \nu \nabla^2 \mathbf{u} + \mathbf{f} \tag{1}$$

$$\mathbf{f}_\epsilon = \mathbf{f} \otimes \eta_\epsilon^{2D}, \quad \eta_\epsilon^{2D}(d) = \frac{1}{\epsilon^2 \pi} \exp[-(d/\epsilon)^2] \tag{2}$$

Aerodynamic forces are calculated by means of look-up tables and the angle of attack is computed using the values taken from the CFD domain through the Effective Velocity Method

(EVM) algorithm, developed by Schito [13]. The EVM is an engineering model tuned on 2D fully resolved CFD numerical campaigns of an isolated airfoil. EVM introduces a correction for the AoA, which undergoes a reduction in proximity of the force concentration region (regularization kernel) due to the downwash caused by the velocity induced by the force distribution of the actuator lines. The expression in Eq.3 highlights the dependence of AoA correction on airfoil chord c and Δ, being the average cell dimension calculated as the cube root of the cell volume within the rotor region. The EVM explicit method requires a convergence on the AoA since C_l depends on $\Delta\alpha$.

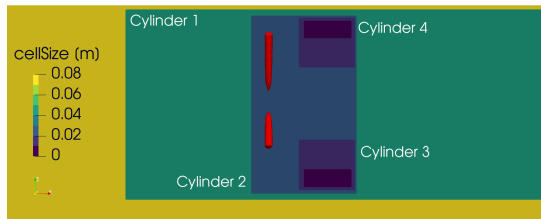$$\Delta\alpha = \alpha_{EVM} - \alpha = \frac{c}{\Delta}(1.2553 - 0.0552 \cdot C_d)\,C_l \qquad (3)$$

The correction $\Delta\alpha$ is subtracted from the averaged sampled α with a probe rake normal to the relative wind speed direction, away 1.5Δ from AL point and 5Δ long. The in-house ALM code features a new FOWT module to impose both surge and pitch motions with respect to the baseline, described in [14], where only surge motion was implemented. The additional degree of freedom of tower pitch is introduced with rigid body motion laws. Furthermore, variable rotational speed Ω and blade collective pitch θ_{pitch} can be given as generic functions of time.

4. CFD-ALM setup

The numerical domain for CFD simulations uses a Cartesian grid and a similar cross section of the wind tunnel; a slip wall condition is selected to avoid the refinement of the wind tunnel boundary layer. The depletion of the height by the boundary displacement thickness of 0.125 m from the bottom and 0.095 m from the top ensures the same wind tunnel mass flow rate [14]. Slip wall condition are applied to lateral walls and no depletion of width is encountered as the blockage is negligible in that direction.

The wake is fully developed in the numerical domain without spurious reflections. Two cylindrical regions (`Cylinder 1` and `Cylinder 2`) enclosing the rotor are refined to solve the wake and the rotor more accurately. Additional annular regions (`Cylinder 3` and `Cylinder 4`) are placed downstream the rotor for a better resolution of the tip vortices to compare results to PIV measurements reported in [15]. The 7.4 million cell mesh has the main purpose to assess the aerodynamic loads, whereas a refined mesh of 25 million cells is adopted for a better resolution of the wake leaving untouched the rotor grid cell size, hence both meshes result in the same rotor loads. The rotor region is embedded into a cylindrical subregion with cell size equal to 0.017 m. Troldborg suggests $R/\Delta = 30$ [2], $R/\Delta = 32$ is used by Forsting [16], Churchfield [17] and Blaylock [18] employ finer grids in the rotor region for NREL Phase VI and NREL 5 MW equal to $R/\Delta \geq 100$ for LES. In the present ALM formulation the number of AL points is constrained by number of cells intersected by the AL, hence the average number of AL points is higher than 75 for surge and pitch simulations. The smearing coefficient $\epsilon/\Delta = 1$ is set in this work, the minimum requirement to solve the Gaussian kernel, as the AoA correction (Eq.3) has been tuned on that value. Troldborg [2] and following studies settle $\epsilon/\Delta \geq 2$ to avoid numerical oscillations in the rotor loads. Although Forsting [19] reports that rotor loads are dependent on ϵ and a proper grid convergence is difficult to achieve. Instead, tighter requirements have been adopted by Martinez-Tossas [20] with $\epsilon/\Delta \geq 5$ finding a negligible change in power.

The unsteady RANS with $k - \omega\ SST$ turbulence closure uses the PISO solver with $\Delta t = 5 \times 10^{-4}$ s so that the blade tip does not exceed one cell per time step, which is more limiting than the Courant number. The time integration is a blended second-order Crank-Nicholson scheme, whereas the interpolation uses the third-order accurate QUICK scheme for advective terms, schemes for Laplacians are Gauss linear corrected. The fixed-bottom load case LC1.1 runs on High Performance Computing (HPC) of Politecnico di Milano equipped with a DELL Intel Xeon Gold 6248 2.50 GHz, 2 $\times$ Intel Xeon Gold 6248 CPUs, 40 system cores, 192 GB RAM, 960 GB SSD drive employing 26 clock hours to simulate $10\,s$ (40 revolutions) on 40 cores.

	Value
Inflow	-11.5 m (4.8D)
Outlet	34.5 m (14.5D)
Side wall	$[-1.65, +1.65]$D
Floor	0 m
Ceiling	3.62 m (1.52D)

Figure 4. Refinement in the rotor region and volume force iso-surface (red). View of xz plane.

Table 2. Dimensions of the numerical domain.

5. Comparative assessment with experiments

The present section reports the experimental validation of the fixed-bottom and floating wind turbine load cases. The experimental campaigns will be referred as Exp.1 and Exp.2 indicating UNAFLOW and follow-on OC6 Phase III campaign, respectively.

5.1. Fixed-bottom wind turbine

LC1.1 steady wind case is simulated for $10\,s$ (40 rotor revolutions) reaching a stationary solution. The ALM stationary solution shows very small oscillations ($< 0.5\%$ of the mean values) of thrust and torque with frequency contents of 1P and multiples and 3P frequency as a consequence of the blockage effect (ratio between rotor swept area and wind tunnel test section area) which induces oscillations of the pressure field generated on the passing blade close to the upper (and lower) wall of the numerical domain. The frequency content of numerical noise equal to 12P is recognized to be linked to the number of AL points since they stem from the grid cells crossed by the actuator line. Experimental raw data features 1P and 2P harmonics, the former ones are ascribed to a mass imbalance of a blade ($\approx 10\%$) exciting 1P blade passing frequency. The latter are related to a plausible aerodynamic imbalance due to a blade pitch error or blade with sensible difference in aerodynamic performances [6]. The tower shadow effect is manifesting with 3P frequency. Therefore, the numerical and experimental results are low-pass filtered at 3 Hz with the aim to maintain only fundamental platform frequencies and neglect the noise at higher frequencies to better get insights from the analyses. ALM thrust is very close to Exp.1 with a percentage error lower than 3%, whereas the torque difference is around 5%. Exp.2 shows lower values, resulting in higher discrepancies with ALM counterparts. The difference between the two experimental campaigns can be due to alternative set-up of the acquisition cabling from load cells placed on the turbine or a small undetected pitch angle of the blades. Previous studies by Cormier *et al.* [21] performed comparative experimental assessment to fully resolved CFD, free vortex wake (FVW) method using lifting line model and BEM on the same test case, neglecting the controlled environment of the wind tunnel. The numerical models show lower thrust and torque as the open field condition does not take into account the blockage of the wind tunnel (around 8%) which would lead to an increased velocity approaching the rotor. Numerical comparisons in [6] suggest a little discrepancy of AoA calculated by the EVM algorithm with respect to FVW model. A small overestimation of the AoA could yield a higher lift, with a major impact on the rotor torque as the lift force projection changes dramatically on the tangential direction with small AoA difference.

5.2. FOWTs

Surge ALM simulations are compared to experiments Exp.1 and Exp.2: surge cases run for 40, 10 and 10 s of simulated time for LC2.1, LC2.5 and LC2.7 respectively to ensure the convergence

**Table 3.** Thrust and torque for LC1.1 and percentage errors.

LC1.1	Thrust [N]	Torque [Nm]
ALM	36.89	3.49
Exp.1	35.91	3.32
% error	+2.74	+5.14
Exp.2	33.68	3.23
% error	+9.52	+8.17

to a periodic solution. It is observed in Fig.5 that the mean thrust F_X and torque M_X are comparable to the experimental values, Exp.2 has a systematic slightly lower values of thrust, instead a nearly halved torque mean is detected for LC2.1. Notwithstanding an uncertainty evaluation is not available for measured data, undoubtedly the latter discrepancies are an issue occurred during the experiment since Exp.1 and Exp.2 have a reasonable agreement for the mean values of the remaining cases. In terms of amplitudes ΔF_X and ΔM_X, ALM thrust agrees with Exp.1 data but LC2.1 tested in Exp.2 still presents an unexpected thrust and torque that result much lower than Exp.1. On the whole, ALM is found widely in accordance to Exp.1 except for the amplitude LC2.7 where a variable response of the rotational speed is encountered during the test due to the non-rigid controller: during the forward pitch the rotational speed increases leading to a nearly doubled torque amplitude. Likewise, a moderate effect is seen also for LC2.5 torque amplitudes. Overall, ALM well predicts thrust and torque mean and amplitude values, but the above said exceptions, with a slight mean value overestimation found in the fixed-bottom case which confirms the hypothesis of a slight under-prediction of the angle of attack. The absence of the tower and nacelle do not represent the cause of the difference between experiments and ALM results as the implementation of the nacelle in the CFD model would increase the overall thrust, amplifying the discrepancy with experimental thrust, whereas the torque should slightly decrease for passive forces involved.
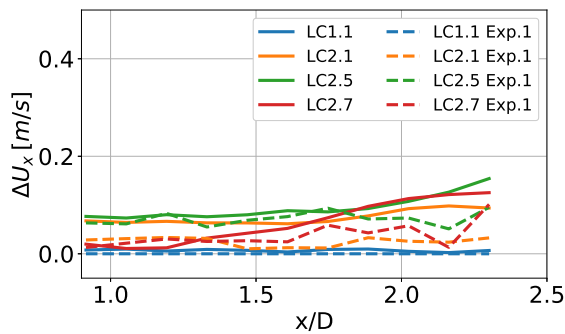
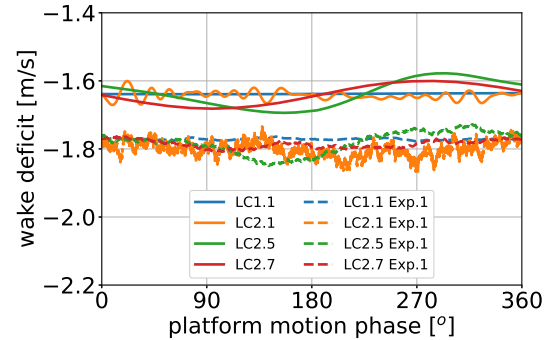Fig.6 shows trends of thrust and torque of pitching FOWTs compared to experiments:
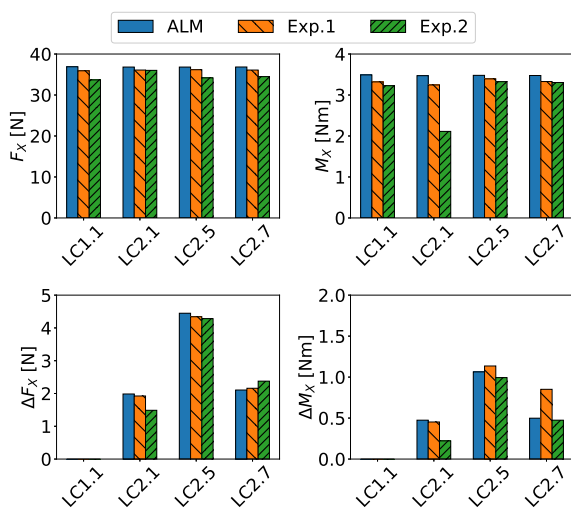
Figure 5. Thrust and torque mean and peak-to-peak values of fixed-bottom and **surge** FOWT.
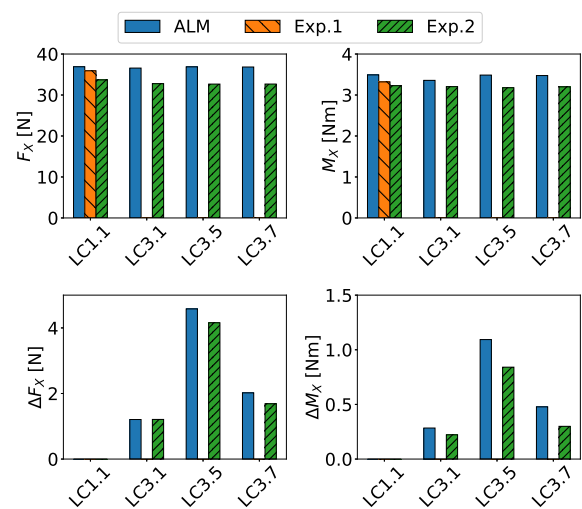
Figure 6. Thrust and torque mean and peak-to-peak values of fixed-bottom and **pitch** FOWT.

Figure 7. Along-wind stream-wise velocity amplitude along the stream-wise direction, y/R=0.75.

Figure 8. Wake deficit over time for fixed-bottom and surge load cases.

Exp.2 presents slightly lower mean ($\approx 12\%$) and peak to peak levels ($\approx 8\%$) compared to ALM. Differences in load amplitudes are observed between ALM and Exp.2 data. The pitch motion induces velocity gradient in the radial direction at the blades, this fairly complicates the estimation of the angle of attack in such a complex flow field. An open discussion is represented by the correlation of the AoA correction applied in the EVM; the tuning of the AoA correction (Eq.3) were based on fixed and plunging airfoil, however a more detailed and flow-based model development is already underway to check the accuracy of the EVM in surge and, especially, pitch motion.

6. Wake analysis

Wake measurements, available by UNAFLOW [22], are compared to ALM outcomes providing a thorough assessment of the medium-fidelity model stating its suitability to solve accurately the wake of a FOWT. The wake assessment is based on the velocity measures carried out with hot wires in stream-wise direction (along-wind, AW) starting from $x/D = 0.9$ up to $x/D = 2.3$ downstream the rotor at a constant $y/R = 0.75$ lying on the plane at hub height. Still, the cross-wind (CW) hot-wire probes measure velocity components at $x/D = 2.3$ along the transversal direction of the wind tunnel flow. OC6 Phase III Definition document [12] summarises the position of the hot-wire probes. The experimental data have been processed performing a phase average with a time window equal to the characteristic surge period whereas only the last surge period of ALM simulations is considered for the comparison.

6.1. Along-wind

Validation of ALM to wake quantities is performed considering the pulsations of the stream-wise velocity due to surge. Stream-wise excursions have been calculated as the difference between the maximum and minimum values of the phase averaged experimental data set. An excellent agreement is fulfilled in Fig.7: the amplification trend of increasing velocity amplitudes is perfectly captured by ALM, made exception for case LC2.1 which estimates twice the experimental velocity amplitude.

6.2. Cross-wind

The transversal hot-wire probe rake sampling at $x/D = 2.3$ provides an estimation of the stream-wise velocity deficit. No alteration of the mean velocity in the wake is detected as the frequency of the surge motion increases. However, the surge motion causes a non negligible oscillations of

wake velocities, hence the wake deficit is studied according to Eq. 4; it implies a higher weight of outboard velocities to outflank the absence of the hub in the ALM simulations.

$$wake\ deficit = \frac{\sum_{i=1}^{n} |r_i| \cdot (U_X - U_0)}{\sum_{i=1}^{n} |r_i|} \tag{4}$$

where r_i is the $i-th$ radius along the cross-wind rake, U_X is the stream-wise velocity component. The wake deficit is evaluated between $y = [-1.6, 1.6]\,m$ along a surge period in Fig. 8. The wake deficit oscillates at the same frequency of the rotor loads. Except for the shift in the wake deficit values which is due to the effect of the nacelle in the experimental campaign, ALM is found in sound agreement with measurements. The wake deficit of the fixed-bottom case stays close to the average value of the surge cases, LC2.5 comparison offers the best match between numerical and experimental data, observing the same locations of its minima and maxima. With increasing frequency, $f = 2\,Hz$, LC2.7 still shows the same wake deficit trend, however the amplitudes are lower and LC2.5 is delayed with respect to LC2.7. Numerical modelling with URANS shows its best predictability for the load cases with higher apparent wind.

7. Near to Far wake analysis

In this section, the far wake analysis with ALM is proposed to study the effects of surge and pitch motions on the mean flow past FOWTs. ALM provided excellent agreements with surge tests and it is considered suitable to model the mean flow with URANS, whereas insightful details on the wake mixing and mitigation are tasks to tackle with a proper LES approach [20]. The stream-wise velocity along the longitudinal extent of the numerical domain through the height of the numerical domain is investigated from $1D$ upstream to $9D$ downstream: mean velocity deficit U_X and normalized standard deviation over a FOWT period are illustrated in Fig.9. For the sake of clarity, $z/D = 0$ denotes the hub height normalized by the diameter since they have two different hub positions.

LC3.5 stands out for the higher wake recovery and shows a non-symmetric 'W' wake profile shape starting from $x/D = 5$ with a higher standard deviation below the hub height, however at $9D$ downstream, the differences of the wake profile reduce. The higher magnitude of the wake recovery is observed in relation with the apparent wind, moreover the pitch motion triggers more recovery than homologous surge case LC2.5. Surge and pitch cases at frequency $f = 1\,Hz$ show the highest variability in terms of standard deviation from $x/D = 3$ downstream, with peaks moving towards the wake core from $x = 3D$ onwards for LC2.5, while the wake instability in LC3.5 moves outwardly the wake core. Increasing frequencies and lower floating displacements make mean velocity profile collapse into the fixed-bottom case. According to the cases studied, the floating motion only provides an enhanced mixing within a limited downstream region with the apparent wind $\Delta V = 0.22$, even though after $9D$ the major differences vanish. Although near wake velocities are widely assessed with URANS to experiments, far wake analysis represent a preparatory stage to Large Eddy Simulations (LES) which is acknowledge as the proper numerical tool to capture the mixing of the turbulent wake behind the wind turbine where URANS are able to catch only the mean flow quantities.

8. Dynamic Inflow Condition

LC2.12 and LC2.17 additional test cases are analysed with ALM numerical tool to test a severe combination of amplitude and frequency of surge displacement and a Dynamic Inflow Control (DIC) strategy [6], reported in Tab.4. This comparison aims at outline the differences and validate the implementation of a collective blade pitch variation imposed to the rotor during FOWT operation using the ALM. In this work a sinusoidal law is imparted with a mean value of 1.5^o in counter phase to the surge motion. This case study mimics a control strategy that realistically takes place in wind farm operation: when apparent wind perceived by the rotor
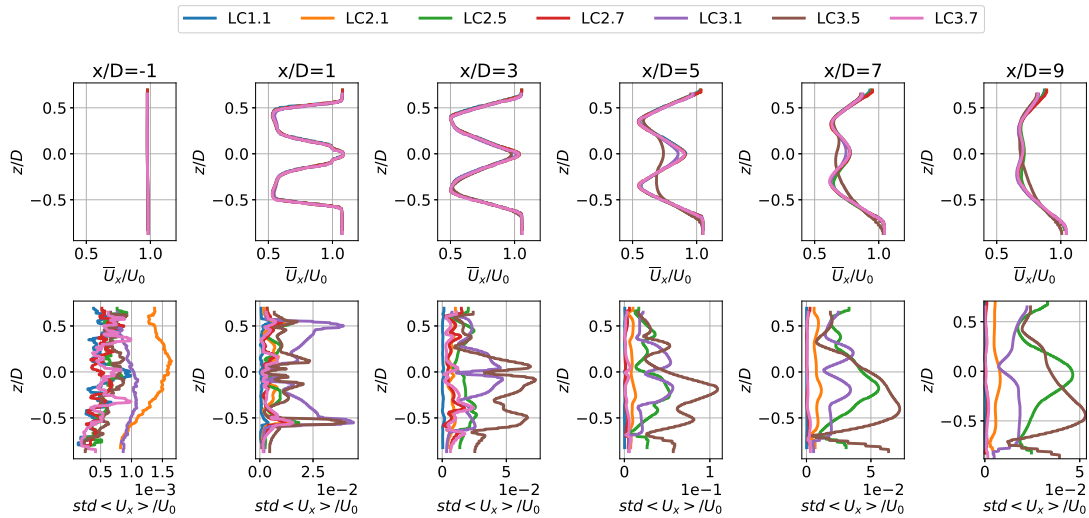
Figure 9. Stream-wise wake velocity and its standard deviation normalized by the free velocity in xy plane for different x/D locations for surge and pitch cases.

Table 4. Surge load cases for DIC simulation.

Load case	U_0 [m/s]	f [Hz]	A [m]/[°]	θ_{shift} [°]	θ_{pitch} [°]
LC2.12	4.0	2.0	0.08	0	
LC2.17	4.0	2.0	0.08	0	1.5 ± 1.5

increases, the control pitches the blades to feather, decreasing the angles of attack hence the aerodynamic loads.
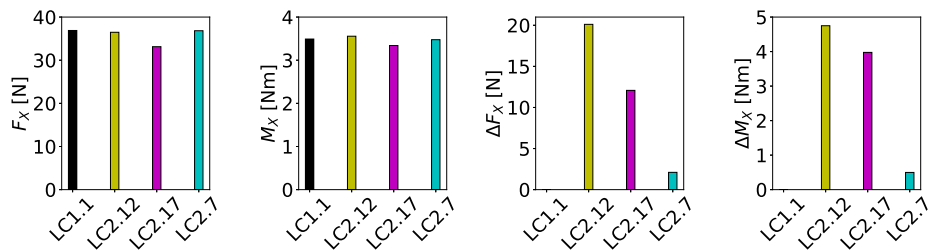
Figure 10. rotor thrust and torque (mean values and amplitudes) of DIC.

In Fig.10, LC1.1 and LC2.7 are reported as comparison since the former represents the fixed-bottom case with no platform motion and the latter has same surge frequency as LC2.12 and LC2.17, LC2.12 has ten times the surge amplitude of LC2.7. Collective pitch targets the load mitigation with respect to LC2.12, halving the thrust force amplitude, preserving the mean torque. The DIC is widely under the spotlight in the wind farm control research aiming at enhancing the wake mixing and recovery so that downstream turbines do not suffer the low momentum contained in the upstream turbine wake. In Fig.11 stream-wise velocities along the z-coordinate demonstrate DIC effects: LC2.17 stream-wise velocity trend stands out at $x = 1D$ and lower wake deficit is visible until $x/D = 9$.
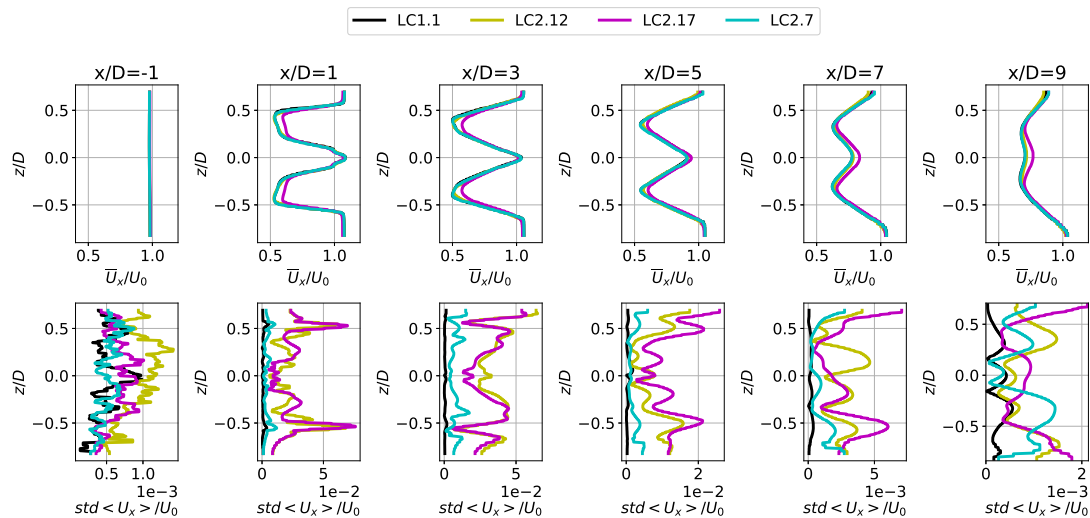
Figure 11. Stream-wise wake velocity and its standard deviation normalized by the free stream velocity in xy plane for different x/D locations applying DIC strategy.

## 9. Flow field: velocity and vorticity

The flow field of stream-wise velocity and vorticity component along y axis are presented in Fig.12, where the wind turbine is moving windward to the free stream wind. First two rows of Fig.12 show load cases LC2.5 and LC3.5, respectively. The complex wake structure of pitching FOWT is observed from $x/D = 4$ onwards. The vortices in the wake of LC3.5 are convected upwards, towards the wake core. The same behaviour is visible in LC2.5 at lower extent, where the vortex sheet amplifies (see vorticity y-component) downstream but they do not break up. LC2.12 and LC2.17 velocity and vorticity fields have similar wake patterns: a higher surge displacement originates wake pulsation from $1D$ rotor downstream and stronger vortices are shed by turbine blade tips. The tip vortex roll-up provokes the so called leapfrogging instability which consists of tip vortex pairing due to fluctuations of convecting velocity in the wake [23]. The simulation with DIC in LC2.17 is characterized by a sensibly lower mean wake deficit respect to LC2.12 demonstrated by quantitative analysis of Fig.11. The leapfrogging instability is better observed in Fig.13, where Q-criterion iso-surface is depicted together with vorticity y-component contours. Despite the low resolution of the numerical domain to limit the computational burden, tip vortices are detected until $x/D = 1$ leaving a fluctuating vortex sheet which suddenly merges into the vortex pairing incorporating tip vortices detached by subsequent blades. Beyond $x/D = 4$, numerical diffusivity smears the vortex rings. The purpose of DIC test is to prove the implementation of sinusoidal blade pitching with URANS to understand the mean flow behaviour with lower resolution discretization to assess the high potential of ALM tool. A proper wake analysis will be addressed with LES approach including details on tip vortex structures.

10. Conclusions

In this paper an in-depth experimental comparative assessment is proposed using an in-house Actuator Line Model featuring the imposed floating motion to simulate the laboratory scale DTU 10 MW wind turbine in surge and pitch. The rotor loads have been found in good agreement with tests performed in the wind tunnel especially in surge motion. Pitch results slightly deviate from experiments, therefore a revision of the ALM velocity sampling, here performed with the engineering EVM correction, will be addressed in the future work to achieve a more general
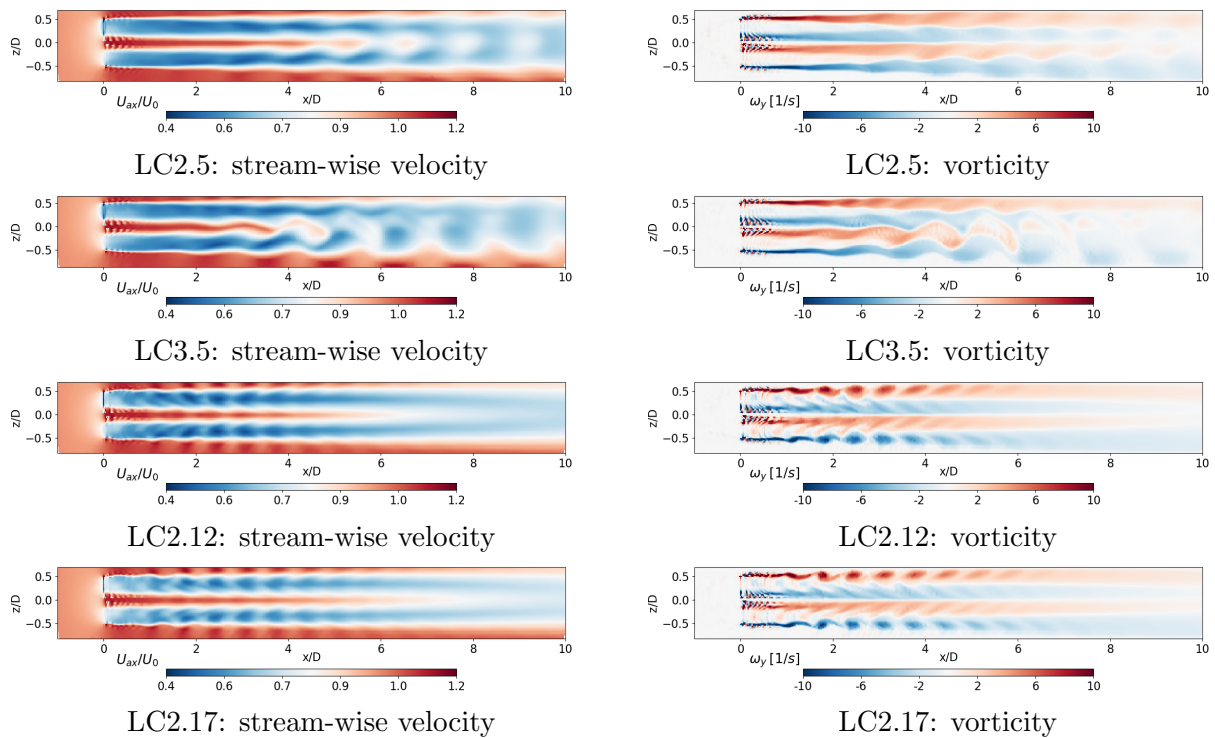
Figure 12. Stream-wise velocity (left column) and y-component vorticity (right column) of xz planes.
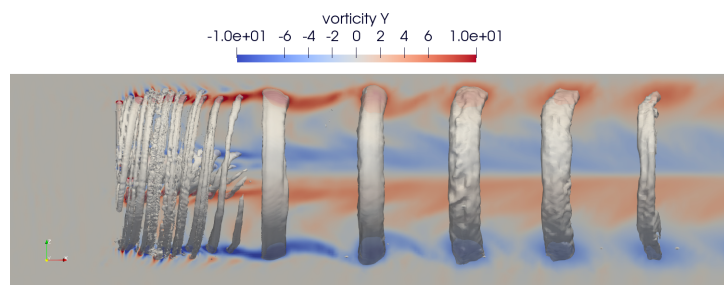
Figure 13. LC2.17: vortex pairing shed by the rotor. Q-criterion iso-surface is visualized in solid white colour and xz slice with vorticity y-component color scale.

formulation suitable for FOWTs. The wake quantities for surge cases are used to validate ALM model in the near wake region, capturing the pulsation of the along- and cross-wind velocity. This allowed to validate the reliability of the ALM which is then used to interpret the far-wake flow behaviour. Further two study cases have been considered with higher surge frequency and amplitude. One of these implements a collective blade pitch control to alleviate the load amplitudes fostering the wake mixing. A flow-field analysis is briefly discussed with emphasis on the vortex pairing occurrence. Overall, the ALM here validated has shown its capability to accurately reproduce both wind turbine loads and wake behaviour. This turns out a fundamental tool in the wind farm simulation which can benefit of lower run times keeping high level of accuracy in the wake region. Ongoing research is also devoted to LES analyses to enhance the understanding of FOWT wake mixing, essential to deal with wind turbine-wake interactions typical of floating wind farms.

References

[1] Sorensen J N and Shen W Z 2002 *Journal of Fluids Engineering* **124** 393–399
[2] Troldborg N 2009 *Actuator Line Modeling of Wind Turbine Wakes* Ph.D. thesis Technical University of Denmark
[3] Mikkelsen R F 2004 *Actuator Disc Methods Applied to Wind Turbines* Ph.D. thesis Technical University of Denmark
[4] Corniglion R, Harris J, Peyrard C and Capaldo M 2020 *Journal of Physics: Conference Series* **1618**
[5] Arabgolarcheh A, Jannesarahmadi S and Benini E 2021 *Renewable Energy* **185** 871–887
[6] Bergua R, Robertson A, Jonkman J, Branlard E, Fontanella A, Belloli M, Schito P, Zasso A, Persico G, Sanvito A *et al.* 2022 *Wind Energy Science Discussions* **2022** 1–33
[7] URL https://a2e.energy.gov/ds/oc6/oc6.phase3
[8] URL https://www.windtunnel.polimi.it/
[9] Bayati I, Belloli M, Bernini L, Boldrin D, Boorsma K, Caboni M, Cormier M, Mikkelsen R, Lutz T and Zasso A 2018 *Journal of Physics: Conference Series* **1037**
[10] Fontanella A, Bayati I, Mikkelsen R, Belloli M and Zasso A 2021 *Wind Energy Science* **6** 1169–1190
[11] Bayati I, Belloli M, LucaBernini and Zasso A 2017 *Journal of Wind Engineering and Industrial Aerodynamics* 217–227
[12] Robertson A, Bergua R, Fontanella A and Jonkman J February 2023 Oc6 phase iii definition document Tech. Rep. NREL/TP-5000-83102 NREL URL https://www.nrel.gov/docs/fy23osti/83102.pdf
[13] Schito P and Zasso A 2014 *Journal of Physics: Conference Series* **524** 012160
[14] Mancini S, Boorsma K, Caboni M, Cormier M, Lutz T, Schito P and Zasso A 2020 *Wind Energy Science* **5** 1713–1730
[15] Cioni S, Papi F, Pagamonci L, Bianchini A, Ramos-García N, Pirrung G, Corniglion R, Lovera A, Galván J, Boisard R, Fontanella A, Schito P, Zasso A, Belloli M, Sanvito A, Persico G *et al.* 2023 *Wind Energy Science Discussions* **2023** 1–37 URL https://wes.copernicus.org/preprints/wes-2023-21/
[16] Forsting A R M, Pirrung G R and Ramos-García N 2019 *IOP Publishing* **1256** 012020
[17] Churchfield M J, Schreck S, Martinez-Tossas L A, Meneveau C and Spalart P R 2017 URL https://www.osti.gov/biblio/1358343
[18] Blaylock M L, Martinez-Tossas L, Sakievich P, Houchens B C, Cheung L, Brown K, Hsieh A, Maniaci D C and Churchfield M J 2022 *AIAA SCITECH 2022 Forum*
[19] Forsting A M and Troldborg N 2020 *Journal of Physics: Conference Series* **1618** 052001
[20] Martínez-Tossas L A, Churchfield M J and Leonardi S 2015 *Wind Energy* **18** 1047–1060
[21] Cormier M, Caboni M, Lutz T, Boorsma K and Krämer E 2018 *Journal of Physics: Conference Series* **1037** 072048
[22] Bayati I, Belloli M, Bernini L and Zasso A 2017 *Energy Procedia* **137** 214–222
[23] Ivanell S, Mikkelsen R, Sørensen J N and Henningson D 2010 *Wind Energy* **13** 705–715 URL https://onlinelibrary.wiley.com/doi/abs/10.1002/we.391